SAXS Measurements of Interfacial Thickness in Amorphous Polymer Blends Containing a Diblock Copolymer

Patrick Perrin and Robert E. Prud'homme*

Centre de recherche en sciences et ingénierie des macromolécules, Chemistry Department, Laval University, Cité Universitaire, Québec, Canada G1K 7P4

Received December 28, 1992; Revised Manuscript Received December 14, 1993

ABSTRACT: Small-angle X-ray scattering measurements were performed in order to estimate the interfacial thickness of melt blended poly(styrene)/poly(methyl methacrylate) samples, with and without the corresponding poly(styrene-*b*-methyl methacrylate) copolymer. The analysis of the scattering profile was based on deviations from Porod's law using the Koberstein/Morra/Stein (*J. Appl. Crystallogr.* **1980**, *13*, 34) graphical method in which the desmearing procedure is avoided. The interfacial thickness was found to increase regularly with the addition of the copolymer, up to 33% when 10 wt % copolymer was added to the homopolymer blend. These results are in agreement with existing theories.

Introduction

Immiscible blends are generally obtained when two homopolymers are mixed together.[1,2] Most often, the resulting material exhibits poor mechanical properties as a result of a weak adhesion between phases. Different procedures have been proposed to stabilize these morphologies. Firstly, an appropriate third homopolymer, miscible with the two others, can be added to the immiscible pair.[3-6] For a sufficiently high content of the third component, miscible ternary blends can be formed. Secondly, a small amount of copolymer, preferentially block or graft copolymer, can be added to the immiscible binary blend. This procedure can be considered as a nonreactive compatibilization method. Thirdly, covalent bonds can be created between two homopolymer phases (reactive compatibilization technique) in order to reinforce the domain boundary.[7] In this paper, we are only concerned with the nonreactive technique with the addition of a block copolymer to an immiscible blend.

Several methods have been used to characterize the morphology of polymer mixtures containing a block copolymer. In a pioneering work, Riess and colleagues[8,9] used the transparency of films cast from solutions as a criterion to appreciate the efficiency of the emulsifying agent. Other studies have focused on the observation of phase size reduction, by scanning and transmission electron microscopies,[10-14] and on the improvement of mechanical properties.[12-14] Direct measurements of the lowering of the interfacial tension were also performed by Anastasiadis et al.[15] Finally, the location of the copolymer at the interface of the immiscible components was successfully verified by Fayt, Jérôme, and Teyssié[16] by dying selectively a short sequence of poly(isoprene) inserted between the two blocks of a poly(styrene-*b*-butadiene) copolymer.

More recently, forward recoil spectrometry was used by Shull et al.[17] to study the diffusion of a poly(styrene-*b*-2-vinylpyridine) copolymer randomly dispersed in the poly(styrene) layer of a poly(styrene)/poly(2-vinylpyridine) bilayer sample. Free copolymer chains were detected at the interface below the critical micelle concentration (ϕ_{cmc}) whereas, above this concentration, copolymer chains were also found at the poly(styrene)/air surface, and micellar segregation at the interface, as confirmed by a direct visualization of the micelles.[18] The molecular arrangement at the interface was studied for the poly(styrene)/poly(methyl methacrylate) (PS/PMMA) system in the absence[19-21] and in the presence[22-24] of a P(S-*b*-MMA) copolymer. Hence, Foster and Wool[21] have measured a value of the interfacial thickness $a_I = 6.0$ nm from welding cleavage experiments. Fernandez et al.[20] have reported, using the method of neutron reflectivity, a value of the interfacial thickness $(2\pi)^{1/2}\sigma = 5.0$ nm (σ is the standard deviation of the Gaussian function used to generate the interface gradient; see eq 10) for spin coated PS/PMMA samples. Similar experiments were conducted by Anastasiadis et al.[19] and a value of $(2\pi)^{1/2}\sigma = 5.4$ nm ($a_I = 5.0$ nm) was reported. Russell et al. have described the composition profile at the interface of PS/PMMA/P(S-*b*-MMA) samples[22,23] and suggested that the interface is saturated with copolymer films of thickness exceeding half the long period of the copolymer. Increasing the thickness of the P(S-*b*-MMA) layer between PS and PMMA to 23.9 nm (these values are smaller than half the copolymer long period of 25.6 nm) causes a gradual increase in the width of the interface from $a_I = 5.0$ to 8.4 nm. Micellar segregation at the interface of these samples was not observed by elastic recoil detection.[24]

The above-mentioned studies give the interfacial thickness of immiscible blends and have permitted a comparison with some of the existing theories. However, a single study deals with mixtures containing a block copolymer at the interface, and the sample investigated in that study was a PS/PMMA bilayer.[22,23] In this article, we have performed SAXS measurements of the width of the segmental profile of PS/PMMA blends prepared from the melt, with and without the corresponding P(S-*b*-MMA) diblock copolymer.

Theoretical Background

a. Binary Homopolymer Morphology. To understand the morphology behavior of amorphous ternary A/B/P(A-*b*-B) blends, a brief overview of some of the advances in the theory of multicomponent polymer systems is now given. Helfand et al.[25-28] have developed quantitative theories which show that decreasing the number of A/B contacts at the interface of an immiscible A/B blend in the molten state involves a decrease of enthalpic and entropic contributions that lead, respectively, to a decrease and an increase of the free energy of the system. The best energetic balance defines the arrangement of the segments at the interface. This concept can easily be understood from the lattice model used by Helfand[28] and Roe[29] who related the interfacial thickness to the interaction pa-

* Abstract published in *Advance ACS Abstracts*, February 15, 1994.

0024-9297/94/2227-1852$04.50/0

rameter, notwithstanding the difficulty of choosing the lattice parameters used in the calculations. The Gaussian random walk model was used by Helfand et al.[25-27] to calculate the interfacial properties in homopolymer blends. In this approach, the polymer chains satisfy a diffusion equation which is modified to take into account the field created by the surrounding chain segments. An analytical solution of the interfacial composition profile, interfacial thickness, $a_{I\infty}$, and interfacial tension, τ_∞, is possible in the limit of infinite chain length, the latter parameter having been recently measured.[30-32] By SAXS, the interfacial thickness is the only measurable parameter and it reads

$$a_{I\infty} = 2\left[\frac{\beta_A^2 + \beta_B^2}{2\chi(\rho_{0A}\rho_{0B})^{1/2}}\right]^{1/2} \quad (1)$$

with

$$\beta_K^2 = (1/6)\rho_{0K} b_K^2 \quad (2)$$

where b_K is the statistical Kuhn segment, ρ_{0K} is the monomer density of component K, and χ is the interaction parameter.

In the square gradient approach initially developed for small molecules,[33] the free energy of a fluctuating system is assumed to depend not only on the local concentration but also on the fluctuations that give an excess free energy. In general, this is expressed as the sum of the Flory–Huggins free energy and a square gradient term. An expression of κ, the coefficient of the square gradient term, was derived by de Gennes[34,35] in the case of polymer molecules using the random phase approximation theory and the linear response theory. In fact, two limiting forms of κ must be considered. The first case corresponds to large wavelength fluctuations in comparison with the chain dimensions and, thus, to a relatively diffuse interface whereas the second case corresponds to short wavelength fluctuations and, hence, to a sharper interface. In both cases, one can write

$$\kappa = \frac{b^2}{\Omega\phi(1-\phi)} \quad (3)$$

where $\Omega = 36$ in the first case and $\Omega = 24$ in the second one. In eq 3, identical chain parameters are assumed and ϕ is the composition of the blend. The interfacial profile is then derived by minimizing the free energy.[36,37] In particular, Broseta et al.[37] have written an expression for a_I:

$$a_I = a_{I\infty}[1 + (1/w_A + 1/w_B)\ln 2] \quad (4)$$

where $w_K = \chi Z_K$, the degree of incompatibility, is assumed to be larger than 5 for eq 4 to be valid. Z_K is the degree of polymerization of component K. This expression goes beyond the usual approximation of infinite molecular weight. As can be seen from eq 4, $a_{I\infty}$ is corrected for entropic effects. Polydisperse systems were also considered by assuming the same bimodal distribution of chain lengths for both the A and B components. As expected, chains of higher molecular weights tend to localize in the bulk phases rather than near the interfacial region. The loss of translational entropy associated with the confinement of the chain into half the space is more easily accepted by large chains than by small ones. A similar behavior was observed for surfaces.[38]

Hong and Noolandi[39] have developed a theory, similar to that of Helfand, for polymer interfaces in A/B blends in the presence of small molecules of solvent which participate to the potential exerted on the K segments (K = A, B) via the polymer–solvent interaction parameters. Finite molecular weights were considered, but excluded volume effects were not addressed by the derivation, this aspect being treated later by Broseta et al.[40] The resulting system of equations can be solved numerically to calculate the interfacial composition profile. As mentioned above, domain boundary thicknesses were measured in PS/PMMA blends.[20,23] Only a few other measurements of the interfacial thickness of A/B blends can be found in the literature.[41-43]

b. Block Copolymer/Homopolymer Morphology. Thermodynamic theories have also been proposed for the morphology of block copolymers. In the disordered state, the thermal concentration fluctuations were characterized whereas, in the ordered state, the size, shape, and interfacial thickness between the microdomains were investigated. Leibler[44] has developed a general theory in the weak segregation regime where the deformation of polymer coils is not significant. In the disordered state, the scattering function was calculated in the context of the random phase approximation, giving a method to measure the interaction parameter between unlike species and to identify the morphology of block copolymers.[45-50] In addition, the microphase separation temperature was predicted and a phase diagram near the transition temperature was determined. Two fundamental parameters were identified: the composition of the copolymer chains, f, and the product of the interaction parameter between species A and B with the total number of repeat units per copolymer chain, χZ_C. For $f = 0.5$, a transition from the disordered state to a lamellar morphology is predicted at $(\chi Z_C)_{transition} \simeq 10.5$. If $f \neq 0.5$, a transition from the disordered state to spherical morphology is expected at values of $(\chi Z_C)_{transition} > 10.5$. Also, at given $(\chi Z_C) > 10.5$ values, the morphology changes from disordered to spherical to cylindrical to lamellar ordered structures as f increases from 0 to 0.5. These different morphologies were observed as early as 1969.[51] Fredrickson and Helfand[52] have extended Leibler's theory and shown that a direct transition from the disordered state to each of the three ordered morphologies is possible by simply changing χZ_C.

In the strong segregation regime, Helfand and Wasserman[53,54] have introduced a theory based on confined chain statistics, where, for a given microdomain geometry (i.e., spherical, cylindrical, or lamellar), the free energy is calculated and minimized. For large χZ_c values, the narrow interface approximation is valid and the microdomain boundary thickness becomes similar to the domain boundary thickness of an A/B mixture (eq 1).[53] Contrary to a_I, the microdomain repeat distance, D, was found to be molecular weight dependent since $D \simeq$ (molecular weight)$^{0.643}$. This result is in agreement with the theory of Otha and Kawasaki[55] who found a $^2/_3$ power law dependency. Experimental measurements of D were performed, and the theoretical predictions were generally confirmed.[56-58] The effect of temperature,[49] molecular weight,[19,56,57,59-62] and sample preparation[59] on the domain boundary thickness was also studied. In general, a_I is found to remain constant upon changing these parameters.

A/P(A-*b*-B) mixtures have also been considered from a theoretical point of view.[63] This system can be described as a block copolymer solution in which the solvent is a preferential macromolecule. The theory allows the calculation of phase diagrams which present interesting features, in particular the observation of an increasing order–disorder transition temperature as the amount of homopolymer increases when $Z_H/Z_C > {}^1/_4$, where Z_H is the degree of polymerization of the homopolymer. Phase diagrams were also investigated experimentally[64,65] as was

the homopolymer-induced mesophase formation.[66] The calculation of the interfacial thickness of A/P(A-*b*-B) mixtures was not performed theoretically, but experimental measurements indicate that the presence of the homopolymer leaves unchanged the domain boundary thickness.[59,64,67-69]

The part of the phase diagram where the concentration of the block copolymer in the mixture is low was studied in detail in separate papers.[70-72] The two models presented by Whitmore and Noolandi,[70] and by Leibler et al.[71,72] are similar in many respects. In both models, the conditions under which spherical micelles can form were investigated and expressions of the critical micelle concentration, $\phi_{cmc}^{spherical}$, were derived. Leibler,[72] for example, gives

$$\phi_{cmc}^{spherical} = \exp[1.72(\chi Z_C)^{1/3} f^{4/9}(1.74 f^{-1/3} - 1)^{1/3} - 1 + Z_C/Z_{HA} - \chi Z_{CB}] \quad (5)$$

with Z_{HA} the degree of polymerization of the homopolymer A and Z_{CB} the degree of polymerization of the B block of the copolymer. The predictions of ϕ_{cmc} were recently extended by Shull et al.[17] to the cases of cylindrical and lamellar micelles. In all cases, geometric parameters like the core radius and the corona thickness can be determined from numerical calculations by assuming that the interfacial thickness between the core and the corona is set equal to $a_{I\infty}$. Micelles were experimentally studied by scattering methods,[73-75] and the theoretical simulations of the resulting scattering curves were successfully performed by assuming either an infinitely sharp boundary thickness or a diffuse interfacial thickness equal to $a_{I\infty}$.

Theories have finally been developed to explain the behavior of A/B/P(X-*b*-Y)/solvent mixtures. For instance, Banaszak and Whitmore[76] have calculated phase diagrams of ternary A/B/P(A-*b*-B) blends. On the other hand, the interfacial thickness of PS/PMMA/P(S-*b*-MMA) blends of high contents of block copolymer and with an equal amount of the two homopolymers was obtained from neutron reflectivity measurements. The microdomain boundary thickness was found to increase by 25% from the pure copolymer to a mixture containing 17% homopolymer.[22] This result is in contrast with previous experiments conducted on A/P(A-*b*-B) blends[59,64,67-69] where the interfacial thickness did not change upon adding the homopolymer. Other studies have focused on the emulsifying effect of block copolymers.[72,77-80] It results from these models that the addition of a block copolymer causes a decrease of the interfacial tension and alters the molecular structure at the interface since a significant penetration of the block copolymer into the homopolymer phases was observed, which results in an enhancement of the adhesion between phases.[81,82] The localization of block copolymer molecules at the interface is responsible for the broadening of the segmental profile, which can be measured experimentally from scattering methods, as shown in this paper. Finally, we should keep in mind that the efficiency of a block copolymer as an emulsifying agent is limited by the formation of micelles in bulk phases and by kinetic factors. Consequently, the block copolymer used as a compatibilizer should be designed by taking many parameters into account (i.e., thermodynamic and kinetic) in order to achieve the desired properties for the mixtures.

c. SAXS Theory. The method used in this paper to determine the interfacial thickness was presented in detail by Koberstein, Morra, and Stein.[83] It involves a graphical analysis of the deviations from Porod's law in which the desmearing procedure is avoided. The limiting behavior of the intensity ($I_{ideal}(s)$) scattered in the Porod region by an ideal two-phase system with sharp boundaries, is described by the Porod relation:[84]

$$\lim_{s\to\infty} \frac{I_{ideal}(s)}{I_e(s)} s^4 = \frac{Q}{2\pi^3 l_c} = K_p \quad (6)$$

where $s = (2 \sin\theta)/\lambda$ is the magnitude of the scattering vector, $I_e(s)$ is the intensity scattered by an electron, Q is the Porod invariant, l_c is the Porod inhomogeneity length, and K_p is the Porod constant. However, in real polymer systems, the product $I_{\mathcal{R}}(s)s^4$ does not reach a constant value. In the limit $s \to \infty$, a modified Porod equation is derived:

$$I_{\mathcal{R}}(s) = I_{ideal}(s)H^2(s) + I_{background}(s) \quad (7)$$

where the limit symbol is omitted for the sake of simplicity. The two terms in eq 7 can be briefly described as follows.

$I_{background}(s)$: The presence of thermal density fluctuations within phases causes positive deviations from Porod's law. Various methods have been presented in the literature to evaluate this contribution.[85-89] In our experiments, the best approach was obtained with the empirical equation developed by Vonk:[89]

$$I_{background}(s) = A + Bs^n \quad (8)$$

where A and B are constants and $n = 2, 4, 6, \ldots$ is an adjustable parameter.

$I_{ideal}H^2(s)$: The diffuse phase boundary is responsible for negative deviations from Porod's law. Vonk[89] and Ruland[90] have shown that Porod's law may be modified to take into account the effect of these deviations with an appropriate model for the electron density gradient across the interface. In this study, a sigmoidal profile was chosen, since it has been justified from thermodynamic considerations,[25,77] where the diffuse electron density profile is suitably described by a convolution product between an ideal electron density profile and a Gaussian smoothing function, $h(r)$. The Fourier transform of the autoconvolution of this electron density profile is given by $I_{ideal}H^2(s)$, and hence, $H(s)$ is the Fourier transform of the Gaussian function $h(r)$ which reads

$$h(r) = (2\pi\sigma^2)^{-1/2} \exp(-r^2/2\sigma^2) \quad (9)$$

where r is a space variable and σ is the standard deviation. σ will be used as a measurement of the diffuse boundary thickness.

Therefore, the scattered intensity if given by

$$I_{\mathcal{R}}(s) - I_{background}(s) = \frac{K_p}{s^4} \exp(-4\pi^2\sigma^2 s^2) \quad (10)$$

This relation is valid with the assumption of a perfect pointlike incident beam. This condition is best approached with pinhole collimation. However, scattering measurements are often carried out using slit collimation of the incident radiation in order to get higher intensity, which leads to the disadvantage that the measured intensity is smeared out and, thus, cannot be compared with eq 10. This problem may be solved by desmearing the scattering intensity. Various desmearing procedures can be found in the literature,[91-95] but the accuracy of these treatments is questionable.[62] Consequently, we have preferred to use the method developed by Koberstein et al.[83] which consists of deriving approximate smeared theoretical relations of the scattered intensity and of analyzing them to determine the interfacial thickness. Guinier and Fournet[96] have calculated an expression for the smeared intensity, $I_{smeared}$:

$$I_{\text{smeared}}(s) = \int_{-\infty}^{\infty}\int_{-\infty}^{\infty} W_l(t) W_w(u) I_{\mathcal{R}}[((s^2 - u^2) + t^2)^{1/2}]\, dt\, du \quad (11)$$

which may be simplified by assuming a negligible contribution of the slit width so that

$$I_{\text{smeared}}(s) = 2\int_0^{\infty} W_l(u) I_{\mathcal{R}}[(s^2 + u^2)^{1/2}]\, du \quad (12)$$

$W_w(u)$ and $W(u)$ are, respectively, the slit-width and the slit-length weighting function and u and t are arbitrary variables of integration. In the context of the Gaussian approximation, $W_k(u)$ (k = l, w) can be written

$$W_k(u) = W_k(0) \exp(-p_k^2 u^2) \quad (13)$$

where $W_k(0)$ is a normalization constant and p_k is related to the standard deviation σ_k of the Gaussian function through the relation $p_k^2 = 1/(2\sigma_k^2)$. Without considering positive deviations and applying eq 12, we have

$$I_{\text{smeared}}(s) = 2W_l(0)K_p \times \exp(p_l^2 s^2)\int_0^{\infty} \frac{\exp[-(p_l^2 + 4\pi^2\sigma^2)(s^2 + u^2)]}{(s^2 + u^2)}\, du \quad (14)$$

Various approximations have been reported to transform this equation into a ready-to-analyze relation. Here we give some of these expressions without discussing the assumptions involved in the calculations.[83] The solution of Ruland[90,97] (extended to the case of a Gaussian weighting function), the exponential solution,[83] the relation of Bonart and Muller,[88] and the empirical solution of Koberstein et al.[83] that fits eq 14, read as follows:

$$I_{\text{smeared}}^{\text{Ruland}}(s) = \frac{K_p'}{s^3} \exp(p_l^2 s^2)(1 - 8\pi^2\alpha^2 s^2) \quad (15)$$

$$I_{\text{smeared}}^{\text{exponential}}(s) = \frac{K_p'}{s^3} \exp(p_l^2 s^2) \exp(-8\pi^2\alpha^2 s^2) \quad (16)$$

$$I_{\text{smeared}}^{\text{Bonart}}(s) = \frac{K_p'}{s^3} \exp(p_l^2 s^2) \exp(-4\pi^2\alpha^2 s^2) \quad (17)$$

$$I_{\text{smeared}}^{\text{empirical}}(s) = \frac{K_p'}{s^3} \exp(p_l^2 s^2) \exp(-38(\alpha s)^{1.81}) \quad (18)$$

In these expressions, $K_p' = 2K_p/(\pi W_l(0))$ and $\sigma = [\alpha^2 - (p_l/(2\pi))^2]^{1/2}$. Suitable plots of these equations allow the determination of σ. In this paper, $E = 12^{1/2}\sigma$ will be taken as a measurement of the domain boundary thickness. This relation was obtained by comparing the Ruland truncated equation with the Vonk expanded form valid for a box smoothing function $h(r)$ (not presented here). This method also requires a self-consistency test for the measurements of the domain boundary thickness, as we will discuss in the Result.

Experimental Section

Table 1 presents the polymers used in this study. All the polymers are amorphous. Molecular weights of PS and PMMA were determined by size exclusion chromatography using μ-Styragel columns and a Waters chromatograph. The measurements were conducted at room temperature in tetrahydrofuran, and the apparatus was calibrated with poly(styrene) standards. The block copolymer P(S-*b*-MMA), synthesized and characterized in the laboratory of Professor Teyssié at the Université de Liège (Belgium), was used as received. The polydispersity of all of these materials is close to unity.

Table 1. Polymers Used

polymer	T_g (°C)	$10^{-3}M_w$	M_w/M_n	source
poly(methyl methacrylate)	124	56	1.14	Polysciences
poly(styrene)	97	57	1.12	Polysar
poly(styrene-*b*-methyl methacrylate) (51 wt % PMMA)	105 and 132	169	<1.09	Liège University (Belgium)

Samples (0.4 g) of polymer (PS, PMMA, and copolymer) were blended from the melt using a Mini Max Molder (Custom Scientific Instruments). The temperature of the mixing chamber was adjusted to 190 °C and the mixing time was 30 min. An injection system allows the extrusion of the melt from a circular aperture of about 2-mm diameter. The samples were molded at 180 °C on a Carver laboratory press and quenched to room temperature while the pressure was maintained to avoid the formation of air bubbles. The samples dimensions were approximately 0.3 × 7 × 32 mm.

Differential scanning calorimetry (DSC) measurements were conducted with a Perkin-Elmer DSC-4 apparatus equipped with a TADS microcomputer. Ultrapure indium was used for DSC calibration. The glass transition temperature, T_g, was recorded at half-height of the corresponding heat capacity jump. After their insertion in the DSC apparatus, all samples were first heated to 433 K for 90 s, quenched to 313 K, and maintained at that temperature for 5 min. A first scan was made at a heating rate of 20 K/min up to 433 K. After quenching, a second scan was performed to assess the reproducibility of the T_g measured values. A third scan was also recorded on some selected samples.

Scanning electron microscopy experiments were conducted with a JEOL Model 840A microscope. This apparatus allows a good resolution at low voltage (5 kV) so that it was possible to study PMMA samples that tend to degrade rapidly under the electron beam. The surface of the sample was smoothed with a Reichert-Jung microtome (Model 2050), and the dispersed phase was extracted by immersion of the sample in a solvent. Cyclohexane was used to extract the PS whereas PMMA was extracted with acetic acid.

SAXS intensity measurements were made with a rotating anode X-ray generator (Rotaflex RU-200 BH, Rigaku-Denki), at a power of 55 kV and 190 mA, with a Ni-filtered Cu Kα radiation used as the incident point focus X-ray source. The wavelength of the radiation is $\lambda = 0.154$ nm. The intensity distribution was measured by a low-angle X-ray camera (Model 2203 E1, Rigaku-Denki) with a step scanning device and a scintillation counter (Model SC-30, Rigaku-Denki). The geometrical parameters of the camera will be given in detail in the paragraph relative to the measurement of the incident beam profile. The intensity was first recorded as a function of the scattering angle (2θ) from $2\theta = -0.4$ to $+0.4°$, with a step interval of 0.01° and a step time of 1 s. It was attenuated by using a set of absorbers so that the scans could be run without damaging the detector. The measured intensity, I_{measured}, was corrected to take into account the detector linearity by applying the relation

$$I_{\text{corrected}} = I_{\text{measured}}/(1 - \tau I_{\text{measured}}) \quad (19)$$

where $\tau = 3 \times 10^{-6}$ s is the response time of the detector. A normalization of the resulting function $I_{\text{corrected}} = f(2\theta)$ was done before comparison with the calculations of Hendricks and Schmidt. The intensity scattered by a sample was recorded from 0.4 to 6°, with a step interval of 0.01 ° and a step time of 120 s. Absorption corrections were not necessary, but the measured intensity distributions were corrected for air scattering before further analysis.

Results

Scanning electron microscopy photographs of PS/PMMA blends containing 30 and 70 wt % PS, with and without the P(S-*b*-MMA) copolymer, were examined, and in both cases, the addition of P(S-*b*-MMA) reduces the size of the phases.[98] In addition, since smaller phases are obtained in blends of high PMMA content, and since it is difficult to analyze the Porod region in blends having

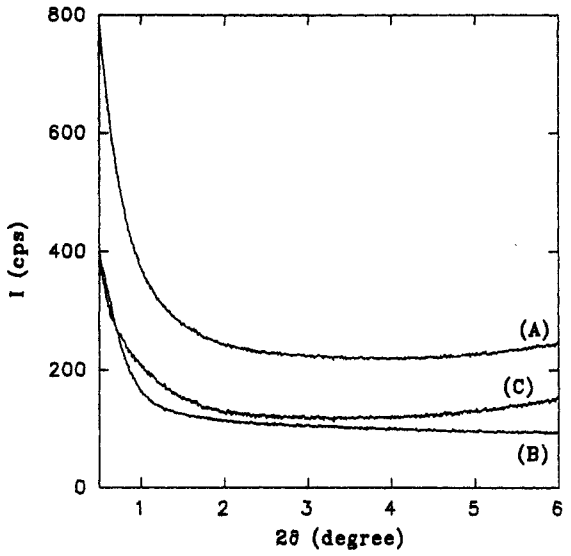

Figure 1. Small-angle X-ray scattering curves: (A) PS/PMMA sample; (B) air; (C) the difference between (A) and (B).

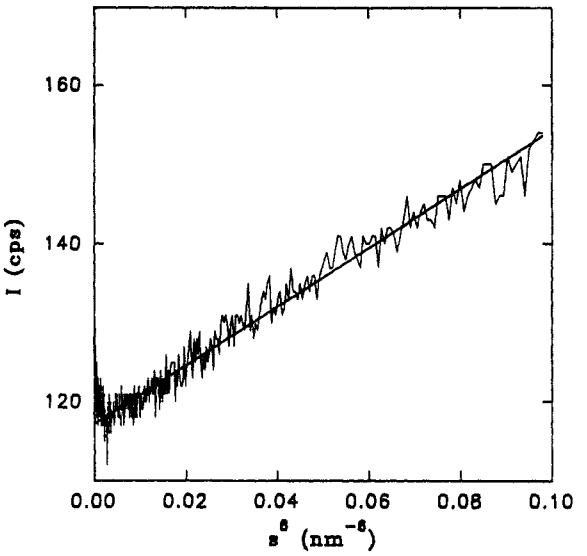

Figure 2. Determination of the background intensity by the empirical Vonk method. The analysis is performed for the PS/PMMA mixture.

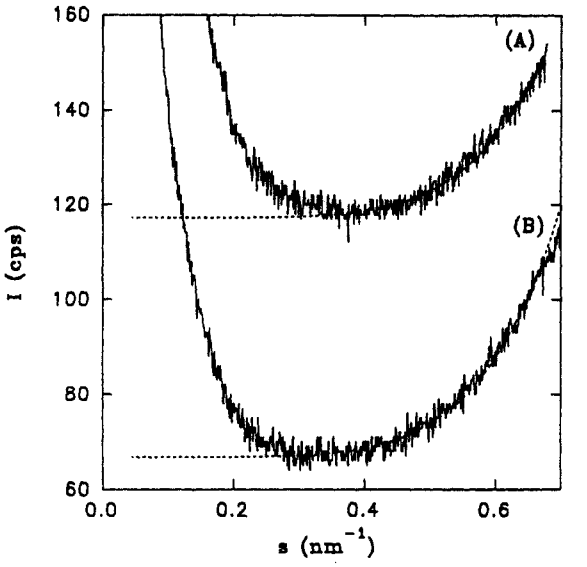

Figure 3. Background intensity determined by the Vonk method for the PS/PMMA mixture without (curve A) and with 10% copolymer (curve B). The scattering curves were not smoothed and curve B was shifted down for clarity.

large phases because the scattered intensity drops off too fast, 30/70 blends only will be considered in what follows, without repeating this composition.

The DSC measurements of PS/PMMA samples containing 0, 2, 5, 10, and 15% copolymer are quite similar. Two T_g's are recorded for each endotherm, and they compare very well with the T_g's of PS and PMMA. These blends are obviously immiscible.[98]

The analysis of the scattering intensity curves requires the determination of the parameter p_l (eq 14) that cannot be directly measured with the Rigaku-Denki collimating system. Nevertheless, $W_k(u)$ was computed from the theoretical method of Hendricks and Schmidt[99] using a Fortran program[100] kindly provided by P. W. Schmidt. In the calculations, the intensity of the focal spot and the sensitivity of the detector were assumed to be uniform. Most of the parameters required to run the program are reported in Appendix 1. The validity of the calculated weighting function $W_l(u)$ was verified indirectly in using the same computer program for the calculations of both the slit-length and the slit-width weighting functions: the measured and calculated $W_w(u)$ functions are in good agreement. Also, the experimental and calculated $W_w(u)$ functions were both fitted with a Gaussian function (eq 13). In both cases, the two curves compare very well to each other.[98] Since the function $W_w(u)$ was measured several times and fitted to a Gaussian function, a mean value of $p_{w\ experimental} = 0.91 \pm 0.01$ mrad^{-1}, with a confidence limit of 95%, is obtained. The fitting of the calculated function $W_w(u)$ leads to a value of $p_{w\ theoretical} = 0.90$ mrad^{-1}. The determination of the interfacial thickness will be performed by taking $p_l = 0$ mrad^{-1}, as explained in the Appendix, but it will be interesting to check the effect of assuming a value of $p_l = 0.02$ mrad^{-1}, this value representing the total height of the error bar calculated from the $p_{w\ experimental}$ values. The validity of the computed slit-length weighting function was also tested by comparing the measured and calculated slit-width weighting functions corresponding to a modified version of the camera. In this experiment, the configuration of the camera was similar except that the widths of the first and second slits were, respectively, equal to 0.08 and 0.06 mm, instead of 0.16 and 0.12 mm in the first case. Again, the agreement between the measured and calculated curves was excellent.[98]

Scattering Curves. Figure 1 shows the intensity scattered by the blend as a function of 2θ (curve A). Curve C, which represents the difference between curve A and the air scattering curve (curve B), was further analyzed to determine the interfacial thickness. The method of Savitsky-Golay (11 points) was retained to smooth out the various scattering intensity distributions; other smoothing methods were tested but no significant change in the value of the domain boundary thickness was found. In addition, the number of iterations in the smoothing procedure of Savitsky-Golay was varied but, again, very slight changes only in the value of the interfacial thickness were observed from the analysis of curves smoothed 0, 1, 5, 10, 50, and 500 times.[98] Nevertheless, 50 times smoothed curves, in addition to unsmoothed curves, will be given because the smoothing is useful in comparison of the data.

Positive Deviations. In our experiments, the background intensity is best described by using the Vonk method with $n = 6$ (eq 8), whatever the amount of copolymer in the blends. The plot of $I(s)$ versus s^6 gives a straight line, as shown in Figure 2 for the mixture, without copolymer. It allows the computation of eq 8, and it clearly appears that the Vonk empirical method fits efficiently the high angle region of the scattering curves (Figure 3). Similar behaviors were found for mixtures containing 2,

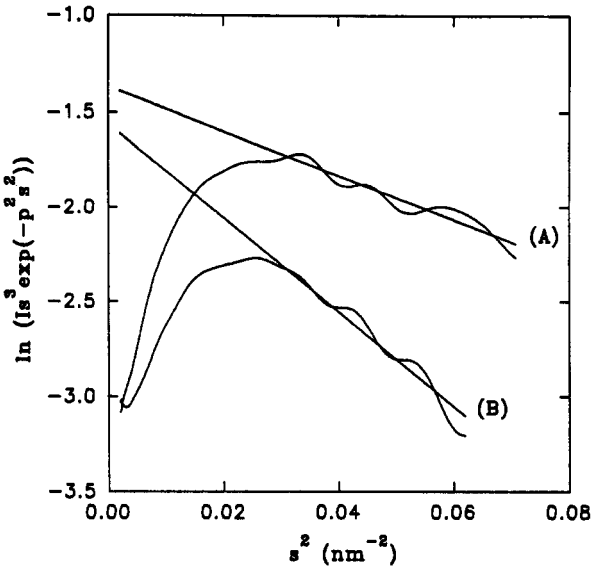

Figure 4. Determination of the interfacial thickness of the PS/PMMA mixture without (curve A) and with 10% copolymer (curve B) by the method of Bonart and by the exponential method. (A) The midpoint is $s = 0.226$ nm^{-1}, $E_{Bonart} = 1.9$ nm and $E_{exponential} = 1.3$ nm. (B) The midpoint is $s = 0.209$ nm^{-1}, $E_{Bonart} = 2.8$ and $E_{exponential} = 1.9$ nm.

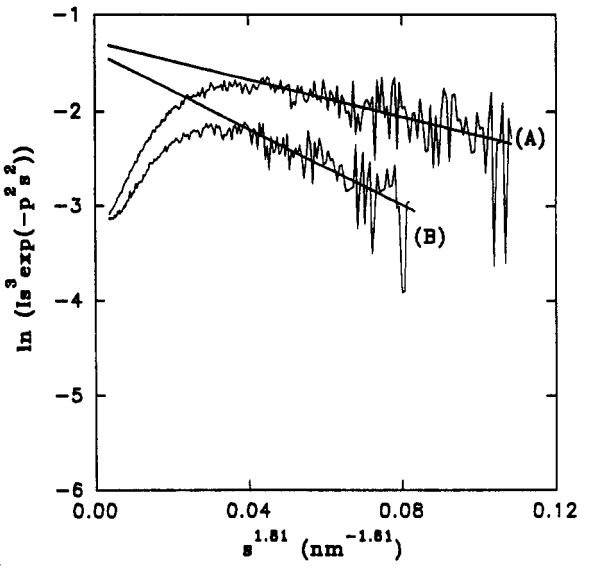

Figure 5. Determination of the interfacial thickness from unsmoothed scattering curves by the empirical method: (A) PS/PMMA mixture without copolymer, $E_{empirical} = 1.6$ nm; (B) PS/PMMA mixture containing 5% copolymer, $E_{empirical} = 2.5$ nm.

5, 10, and 15% copolymer.[98] The subtraction of the background intensity can therefore be performed, and the resulting scattered intensity can be used to evaluate the domain boundary thickness.

Estimation of the Interfacial Thickness. The analysis of the mixtures, with and without 10% copolymer, was made with the Bonart, empirical, and Ruland methods.[98] The determination of the domain boundary thickness requires the same graphical analysis for both the Bonart and the exponential methods (eqs 17 and 16). Consequently, a single plot is presented in Figure 4 for these two methods. A linear regression is performed on the linear angular range from which the slope and, thus, the interfacial thickness, E, are finally calculated. The graphical method of Bonart yields a value $E_{Bonart} = 1.9$ nm, whereas the exponential approach leads to $E_{exponential} = 1.3$ nm for blends without copolymer (Figure 4). The mixture with 10% copolymer gives $E_{Bonart} = 2.8$ nm and $E_{exponential} = 1.9$ nm. For the empirical (eq 18) and Ruland (eq 15) plots, the corresponding E values are $E_{empirical} = 1.6$ nm, $E_{Ruland} = 1.1$ nm, $E_{empirical}$ (10%) = 2.5 nm, and E_{Ruland} (10%) = 1.3 nm.[98] As expected, the inequality $E_{Ruland} < E_{exponential} < E_{empirical} < E_{Bonart}$ is satisfied. The same analysis was successfully performed on blends containing 2, 5, and 15% copolymer.[98] As an illustrative example, Figure 5 gives the empirical analysis of unsmoothed scattering curves of blends containing 0 and 5% copolymer. It clearly shows that the differences observed in the slopes are not due to smoothing artifacts and are well beyond the experimental errors.

As mentioned in a previous section, several approximations are involved in the derivations of eqs 15–17 and, therefore, the values of the interfacial thickness computed by these various methods are different from the true value, E_{true}, obtained from eq 14. The domain boundary thickness value calculated by the empirical method (eq 18) is obviously the closest to the true value, since as shown by Koberstein et al.,[83] the two values are similar within 5% error on a broad range of σs. Therefore, we have assumed that $E_{empirical} = E_{true}$. This approximation has avoided the use of the "cubic spline function derivative estimator routine",[101] since the first derivative of $\exp(-38s^{1.81})$ with respect to s^2 can be calculated analytically. Consequently, the calculation of the self-consistency test diagram, shown

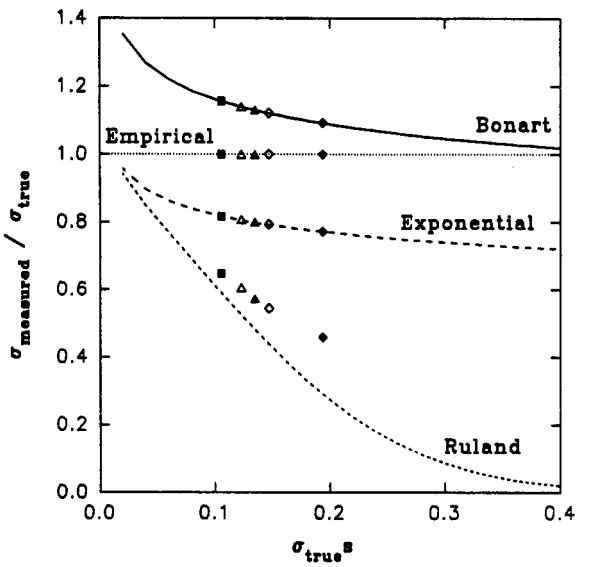

Figure 6. Self-consistency test diagram for the determination of the interfacial thickness by graphical methods in PS/PMMA mixtures containing various amounts of copolymer: (■) 0%; (△) 2%; (▲) 5%; (◇) 10%; (◆) 15%.

in Figure 6, was considerably simplified. It shows a good agreement between all measurements, except for slight deviations recorded for the method of Ruland, confirming the validity of the analysis.

For all the samples, the values of the interfacial thickness obtained from the empirical method are reported in Table 2. Two samples were prepared for each composition, and each sample was scanned three times. From the six measurements, an average value, $E_{average}$, was calculated and is reported in Figure 7 and in Table 2. However, for the mixture containing 15% copolymer, only two measurements on the same sample were performed, leading to a similar value of 3.2 nm. Consequently, no error bar is indicated on Figure 7 for this particular sample. For the other ones, a confidence limit of 95% is given for the calculation of the error. The effect of the parameter p_1 on the domain boundary thickness was also studied. For example, the empirical analysis of the blend was performed by taking $p_1 = 0.02$ mrad^{-1} instead of 0.00 mrad^{-1}, as explained above. A value of $E_{empirical} = 1.5$ nm is then extrapolated as compared to the value of 1.6 nm calculated previously, the difference being smaller than the error bar

Table 2. Empirical Measurements of the Interfacial Thickness, E, in PS/PMMA (30/70) Mixtures Containing Various Amounts of Copolymer

sample	E (0%) (nm)			E (2%) (nm)			E (5%) (nm)			E (10%) (nm)			E (15%) (nm)	
1	1.5	1.6	1.8	2.0	2.1	1.9	2.2	2.4	2.1	2.5	2.5	2.4	3.2	3.2
2	1.9	1.7	2.1	2.2	1.9	2.0	2.2	2.5	2.5	2.4	2.3	2.3		
	E_{av} = 1.8 nm			E_{av} = 2.0 nm			E_{av} = 2.3 nm			E_{av} = 2.4 nm			E_{av} = 3.2 nm	

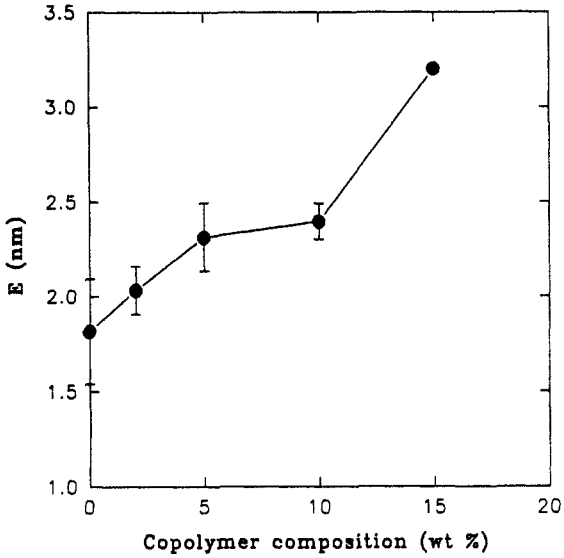

Figure 7. Variation of E with the copolymer composition in PS/PMMA mixtures.

indicated on Figure 7. In addition, the various measurements of the interfacial thickness are shifted by the same number when a different p_1 parameter is used, such that the comparison of the measured values of E of blends of different compositions remains unchanged. As a conclusion, the width of the segmental density profile at the interface broadens as the copolymer is added to the PS/PMMA blend.

Discussion

In this study, the addition of 5% copolymer was necessary in order to observe a significant reduction of the size of the dispersed phase. In addition, the 30/70 blend containing 5% copolymer exhibits an interfacial thickness significantly larger than that of the mixture of the homopolymers. These observations are consistent with the lowering of the interfacial tension as the copolymer goes to the interface. The interfacial thickness is found to increase by 33% when 10 wt % copolymer is added to the blend (and by 78% with 15% copolymer). This result is qualitatively in agreement with that of Russell et al.[22,23] where a maximum increase of 68% (a_I = 5.0 nm without copolymer and a_I = 8.4 nm with copolymer) was measured by neutron reflectivity of spin coated samples. However, the values of the interfacial thickness found in this study, varying between 1.8 and 3.2 nm, indicate a relatively sharp domain boundary zone whereas the measurements of Russell et al.[22,23] and those of Fernandez et al.[20] indicate a more diffuse interface. There is not necessarily a contradiction between the two sets of values since the two approaches, and particularly the methods of sample preparation, are very different. For example, thermodynamic equilibrium conditions may not have been reached in any of these two cases, but the two samples may have evolved differently in that direction. We also note that a wide range of interfacial thickness values have been reported recently for various immiscible systems. Ellipsometric measurements of PS/PMMA blends give values ranging between 2 and 8 nm in one case[102] and values close to 3 nm, at 140 °C, in a second one.[103] Two series of results have also been published for mixtures of PS with poly(*p*-bromostyrene). Values of 1.3 nm were found in a first study by X-ray reflectometry,[104] whereas a comparison between X-ray and neutron reflectometry leads to 3.9 ± 0.5 nm in the first case and 4.1 ± 0.5 in the second one.[105]

As reviewed in the Introduction, the broadening of the interfacial segment density profile in the presence of a copolymer can only be determined by solving numerically a set of equations. These calculations were not made in this study but eqs 1 and 4 were used to obtain the domain boundary thickness in the absence of a copolymer. A similar value of the statistical Kuhn segment was taken for both PS and PMMA, as suggested by Russell et al.,[22] such that $b_{PS} = b_{PMMA} = 0.685$ nm.[106-108] The monomer densities of PMMA and PS were respectively calculated from the density of PMMA at 190 °C, ρ_{PMMA} (190 °C) = 1.08 g/cm^3, and from the density of PS at 190 °C, ρ_{PS} (190 °C) = 0.97 g/cm^3. These values were obtained by using the relationship $v_{sp}(T) = v_{sp}(T_0)e^{\alpha(T)\Delta T}$ where $v_{sp}(T)$ and $\alpha(T)$ are respectively the specific volume and the thermal expansion coefficient at temperature T. α_{PS}(135 °C) and $v_{sp\ PS}$(135 °C) were reported by McMaster,[109] while α_{PMMA}(120 °C) and $v_{sp\ PMMA}$(120 °C) were given by Rogers and Mandelkern.[110] The degrees of polymerization are $Z_{H\ PS}$ = 548 and $Z_{H\ PMMA}$ = 560. The variation of $\chi_{PS/PMMA}$ as a function of the temperature was studied by Russell et al.[50] and a value of 0.0364 was used in our calculations. Hence, we obtained $a_{I\infty}$ = 2.9 nm and a_I = 3.1 nm, i.e., E_∞ = 4.4 nm and E = 4.7 nm. These theoretical values are larger than those measured herein (but smaller than those reported by Russell et al.).

Let us consider now the limits of validity of our analysis. Firstly, the empirical evaluation of the positive deviations may certainly be regarded as a critical step. In order to estimate the background intensity, a range of angles up to $2\theta_{max} = 6°$ was chosen because we have observed that the fitting in the high angle region of the scattering curves is better with $2\theta_{max} = 6°$ than with other values. If the full analysis is carried out with $2\theta_{max} = 7°$, the interfacial thickness $E_{empirical}$ equals 2.2 nm instead of 1.6 nm (see Table 2, sample 1, second scan) without copolymer and 3.8 nm instead of 2.5 nm (Table 2, sample 1, first and second scans) with 10% copolymer. The same analysis with $2\theta_{max} = 5°$ gives 1.4 nm without copolymer and 2.2 nm with 10% copolymer. Consequently, the interfacial thickness is found to depend on the estimation of the background intensity but in all cases a larger value of E is measured for mixtures containing copolymer. The careful analysis of $I_{background}$ was practically conducted as follows. The largest possible value of $2\theta_{max}$ was chosen so that the best fit by the Vonk method could be obtained in the region of high angles, i.e. in Figure 3, as well as the most appropriate self-consistency test diagram (Figure 6).

In our analysis, the possible formation of micelles was implicitly neglected. Using various micellar theories,[17,70-72] the critical micelle concentration of copolymer in the PS matrix was determined, leading to ϕ_{cmc}(spheres) = 3.61 × 10^{-11} (eqs 5)[72] to ϕ_{cmc}(cylinders) = 2.52 × 10^{-11},[17] and to ϕ_{cmc}(lamellae) = 1.65 × 10^{-11}.[17] Assuming an ideal behavior of the PS block (micelle corona), a value of ϕ_{cmc}(spheres) = 3.65 × 10^{-11} was calculated with the theory of Whitmore and Noolandi.[70] The critical micelle concentration of

copolymer in the PMMA matrix was similarly computed giving $\phi_{cmc} \simeq 10^{-10}$, whatever the theory and the geometry of the micelles. These values are rigourously valid for the binary P(S-*b*-MMA)/PS and P(S-*b*-MMA)/PMMA systems. In ternary PS/PMMA/P(S-*b*-MMA) blends, the copolymer chains have the possibility of localizing at the interface, such that a larger amount of copolymer would probably be tolerated before the formation of the micelles occurs. However, it appears from the calculations that the micelles can form even at a low copolymer concentration.

It may also be interesting to consider the surface occupied by a copolymer chain at the interface, Σ, by using a relationship suggested by Paul:[111]

$$\Sigma = \phi_{PS} M/(\rho_{blend} WR(6.023 \times 10^{23})) \quad (20)$$

where M is the molecular weight of the copolymer, ϕ_{PS} is the volume fraction of the dispersed phase, R is the radius of the PS spheres, ρ_{blend} is the density of the blend, and W is the weight fraction of copolymer required to saturate the interface. From scanning electron microscopy pictures,[98] the largest radius of the spheres was measured for the 30/70 blend containing 15% copolymer which has a value of $R = 0.136\ \mu m$. Using eq 20 leads to $\Sigma = 10.6\ nm^2$, which is larger than the minimum possible value, $\Sigma = 0.50\ nm^2$, given by Paul[111] and close to the value, $\Sigma = 9.95\ nm^2$, determined experimentally by Russell et al.[23] from the measurement of the copolymer density profile at the PS/PMMA interface. It can then be concluded from steric considerations that all the copolymer chains can be located at the interface whereas micelles have certainly formed from a thermodynamic point of view. However, in a real situation where the kinetic effects occur, the copolymer chains can remain free in the bulk phases or they can aggregate to form micelles or diffuse at the interface, such that the resulting morphology can be quite complex. The segregation of the micelles at the interface is also possible.

Information regarding the micellar structure can be obtained at angles smaller than those of the Porod region, without perturbing the analysis of the interfacial thickness, but the presence of micelles could not be detected in this study from X-ray scattering, even at low angles by using smaller slits. On the other hand, if we assume that the scattering contribution in the Porod region of the core–corona interface is not too weak to be detected, the reported values of E must be considered as an average of all the diffuse domain boundary thicknesses in the mixture. Since, as mentioned in the Introduction, the diffuse boundary thickness of micelles is normally taken equal to $a_{I\infty}$,[73-75] the interfacial thickness measured in this paper for mixtures containing copolymer chains could be consequently smaller than the real thickness of the PS/PMMA interface. Hence, the addition of 10% copolymer in the 30/70 blend might have caused an increase of the interfacial thickness larger than the measured increase of 33%.

Conclusion

The variation of the interfacial thickness of PS/PMMA mixtures as a function of the added amount of P(S-*b*-MMA) copolymer was studied by SAXS measurements. As expected from the theory, an increase in the width of the segmental density profile and a reduction in the size of the dispersed phase was observed with the addition of the copolymer. An increase of 33% was recorded for the 30/70 mixture with the addition of 10% copolymer, from an initial value of 1.8 nm to a final value of 2.4 nm. As shown in this paper, the measurement of the interfacial thickness by SAXS can be made on samples prepared by melt blending or under any other industrial process. However, it requires the determination of the weighting functions and an accurate estimation of the positive deviations from Porod's law. Finally, as is the case in all scattering methods, the interpretation of the results requires some assumptions regarding the morphology of the samples.

Acknowledgment. We thank the Natural Sciences and Engineering Research Council of Canada and the Department of Education of the Province of Quebec (FCAR and Action structurante programs) for the grants that supported this study. S. Dallaire is acknowledged for providing the software for the analysis of the X-ray curves. We finally thank Dr. P. W. Schmidt for having sent us the Fortran program for the evaluation of the weighting functions.

Appendix 1

In calculating the weighting functions $W_l(u)$ and $W_w(u)$ using the method of Hendricks and Schmidt,[99,100] the geometry of the SAXS camera needs to be specified precisely. With respect to the nomenclature used in the computer method, the following data were used for the slit width weighting function $W_w(u)$: $D(1) = D(2) = 12.5$ mm, $D(3) = D(4) = 58$ mm, $D(5) = D(6) = 160$ mm, $D(7) = D(8) = 260$ mm, $H(1) = H(2) = 0.12$ mm, $H(3) = H(4) = 0.06$ mm, $H(5) = H(6) = 0.08$ mm, and $H(7) = H(8) = 0.5$ mm, for the slits located between the sample and the source planes (labeled by the subscript i in the program), where the $D(i)$'s are distances from the sample plane to the plane perpendicular to the incident beam and containing the edge of the slits and the $H(i)$'s represents the half-widths of the slits. Similary, for the slits between the sample and the detector planes (labeled by the index j in the program) $D(1) = D(2) = 245$ mm, $D(3) = D(4) = 329$ mm, $D(j \geq 5) = 0$, $H(1) = H(2) = 0.1$ mm, $H(3) = H(4) = 2$ mm, and $H(j \geq 5) = 0$. Finally, the sample to detector distance is 355 mm, the sample to focal spot distance is 260 mm, and the receiving slit width is 2×0.1 mm. For the calculation of the slit length weighting function $W_l(u)$, the values of $D(i)$ and $D(j)$ are similar to those used for the determination of $W_w(u)$ but the $H(k)$ values ($k = i, j$) are different. The $H(i)$'s are given by $H(1) = H(2) = 17.5$ mm, $H(3) = H(4) = 10$ mm, $H(5) = H(6) = 8$ mm, $H(7) = H(8) = 0.25$ mm, and for $H(j)$: $H(1) = H(2) = 11$ mm, $H(3) = H(4) = 10$ mm, and $H(j \geq 5) = 0$. Finally, the receiving slit length is 2×9 mm. The output data also give the maximum angle for which the infinite beam approximation is valid, $2\theta_{maximum} = 60.78$ mrad. Therefore, a value of $p_l = 0\ mrad^{-1}$ is used in the analysis of the scattering curves and eqs 16–19 reduce to their corresponding infinite slit height equations.

References and Notes

(1) Paul, D. R.; Newman, S. *Polymer Blends*; Academic Press: New York, 1978; Vol. 1.
(2) Krause, S. Reference 1, Chapter 2.
(3) Perrin, P.; Prud'homme, R. E. *Acta Polym.* **1993**, *44*, 307.
(4) Ameduri, B.; Prud'homme, R. E. *Polymer* **1988**, *29*, 1052.
(5) Champagne, M.; Prud'homme, R. E. *J. Polym. Sci., Part B: Polym. Phys.*, in press.
(6) Christiansen, W. H.; Paul, D. R.; Barlow, J. W. *J. Appl. Polym. Sci.* **1987**, *34*, 537.
(7) Xanthos, M. *Polym. Eng. Sci.* **1982**, *28*, 1392.
(8) Riess, G.; Kohler, J.; Tournut, C.; Banderet, A. *Makromol. Chem.* **1967**, *101*, 58.
(9) Banderet, A.; Tournut, C.; Riess, G. *J. Polym. Sci.* **1967**, *C16*, 2601.
(10) Ouhadi, T.; Fayt, R.; Jérôme, R.; Teyssié, Ph. *J. Appl. Polym. Sci.* **1986**, *32*, 5647.
(11) Jo, W. H.; Kim, H. C.; Baik, D. H. *Macromolecules* **1991**, *24*, 2231.

(12) Fayt, R.; Teyssié, Ph. *Polym. Eng. Sci.* **1990**, *30*, 937.
(13) Heuschen, J.; Vion, J. M.; Jérôme, R.; Teyssié, Ph. *Polymer* **1990**, *31*, 1473.
(14) Sakellariou, P.; Eastmond, G. C.; Miles, I. S. *Polymer* **1991**, *32*, 2351.
(15) Anastasiadis, S. H.; Gancarz, I.; Koberstein, J. T. *Macromolecules* **1989**, *22*, 1449.
(16) Fayt, R.; Jérôme, R.; Teyssié, Ph. *J. Polym. Sci., Polym. Lett. Ed.* **1986**, *24*, 25.
(17) Shull, K. R.; Kramer, E. J.; Hadziioannou, G.; Tang, W. *Macromolecules* **1990**, *23*, 4780.
(18) Shull, K. R.; Winey, K. I.; Thomas, E. L.; Kramer, E. J. *Macromolecules* **1991**, *24*, 2748.
(19) Anastasiadis, S. H.; Russell, T. P.; Satija, S. K.; Majkrzak, C. F. *Phys. Rev. Lett.* **1989**, *62*, 1852; *J. Chem. Phys.* **1990**, *92*, 5677.
(20) Fernandez, M. L.; Higgins, J. S.; Penfold, J.; Ward, R. C.; Shackleton, C.; Walsh, D. J. *Polymer* **1988**, *29*, 1923.
(21) Foster, K. L.; Wool, R. P. *Macromolecules* **1991**, *24*, 1397.
(22) Russell, T. P.; Menelle, A.; Hamilton, W. A.; Smith, G. S.; Satija, S. K.; Majkrzak, C. F. *Macromolecules* **1991**, *24*, 5721.
(23) Russell, T. P.; Anastasiadis, S. H.; Menelle, A.; Felcher, G. P.; Satija, S. K. *Macromolecules* **1991**, *24*, 1575.
(24) Green, P. F.; Russell, T. P. *Macromolecules* **1991**, *24*, 2931.
(25) Helfand, E.; Tagami, Y. *Polym. Lett.* **1971**, *9*, 741; *J. Chem. Phys.* **1971**, *57*, 1812; *Ibid.* **1972**, *56*, 3592.
(26) Helfand, E. *J. Chem. Phys.* **1975**, *62*, 999.
(27) Helfand, E.; Sapse, A. M. *J. Chem. Phys.* **1975**, *62*, 1327.
(28) Helfand, E. *J. Chem. Phys.* **1975**, *63*, 2192.
(29) Roe, R. J. *J. Chem. Phys.* **1975**, *62*, 490.
(30) Anastasiadis, S. H.; Chen, J. K.; Koberstein, J. T.; Sohn, J. E.; Emerson, J. A. *Polym. Eng. Sci.* **1986**, *26*, 1410.
(31) Anastasiadis, S. H.; Gancarz, I.; Koberstein, J. T. *Macromolecules* **1988**, *21*, 2980.
(32) Wu, S. *Polym. Eng. Sci.* **1987**, *27*, 335. Reference 1, Chapter 6.
(33) Cahn, J. W.; Hilliard, J. E. *J. Chem. Phys.* **1958**, *28*, 258.
(34) de Gennes, P. G. *J. Phys.* **1970**, *31*, 235.
(35) de Gennes, P. G. *Scaling Concepts in Polymer Physics*; Cornell University Press: Ithaca, NY, and London, 1979.
(36) Binder, K.; Frisch, H. L. *Macromolecules* **1984**, *17*, 2928.
(37) Broseta, D.; Fredrickson, G. H.; Helfand, E.; Leibler, L. *Macromolecules* **1990**, *23*, 132.
(38) Hariharan, A.; Kumar, S. K.; Russell, T. P. *Macromolecules* **1990**, *23*, 3584.
(39) Hong, K. M.; Noolandi, J. *Macromolecules* **1980**, *13*, 964; **1981**, *14*, 727, 736.
(40) Broseta, D.; Leibler, L.; Kaddour, L. O.; Strazielle, C. *J. Chem. Phys.* **1987**, *87*, 7248.
(41) Wlochowicz, A.; Janicki, J. *J. Appl. Polym. Sci.* **1989**, *38*, 1469.
(42) Janicki, J.; Wlochowicz, A.; Rabiej, St. *Acta Polym.* **1986**, *37*, 229.
(43) Foster, M.; Stamm, M.; Reiter, G.; Huttenbach, S. *Vacuum* **1990**, *41*, 1441.
(44) Leibler, L. *Macromolecules* **1980**, *13*, 1602.
(45) Mori, K.; Tanaka, H.; Hasegawa, H.; Hashimoto, T. *Polymer* **1989**, *30*, 1389.
(46) Mori, K.; Hasegawa, H.; Hashimoto, T. *Polym. J.* **1985**, *17*, 799.
(47) Owens, J. N.; Gancarz, I. S.; Koberstein, J. T. *Macromolecules* **1989**, *22*, 3380.
(48) Bates, F. S.; Hartney, M. A. *Macromolecules* **1985**, *18*, 2478.
(49) Roe, R. J.; Fishkis, M.; Chang, J. C. *Macromolecules* **1981**, *14*, 1091.
(50) Russell, T. P.; Hjelm, R. P.; Seeger, P. A. *Macromolecules* **1990**, *23*, 890.
(51) Inoue, T.; Soen, T.; Hashimoto, T.; Kawai, H. *J. Polym. Sci.* **1969**, *A2*, 7, 1283; *Macromolecules* **1970**, *3*, 87.
(52) Fredrickson, G. H.; Helfand, E. *J. Chem. Phys.* **1987**, *87*, 697.
(53) Helfand, E. *Macromolecules* **1975**, *8*, 552.
(54) Helfand, E.; Wasserman, Z. R. *Macromolecules* **1976**, *9*, 879; **1978**, *11*, 960; **1980**, *13*, 994.
(55) Ohta, T.; Kawasaki, K. *Macromolecules* **1986**, *19*, 2621.
(56) Hashimoto, T.; Fujimura, M.; Kawai, H. *Macromolecules* **1980**, *13*, 1660.
(57) Hashimoto, T.; Shibayama, M.; Kawai, H. *Macromolecules* **1980**, *13*, 1237.
(58) Matsushita, Y.; Mori, K.; Saguchi, R.; Naka, Y.; Noda, I.; Nagasawa, M. *Macromolecules* **1990**, *23*, 4313.
(59) Bates, F. S.; Berney, C. V.; Cohen, R. E. *Macromolecules* **1983**, *16*, 1101.
(60) Hashimoto, T.; Todo, A.; Itoi, H.; Kawai, H. *Macromolecules* **1977**, *10*, 377.
(61) Todo, A.; Miyoshi, K.; Hashimoto, T.; Kawai, H. *Polym. Eng. Sci.* **1977**, *17*, 587.
(62) Todo, A.; Hashimoto, T.; Kawai, H. *J. Appl. Crystallogr.* **1978**, *11*, 558.
(63) Whitmore, M. D.; Noolandi, J. *Macromolecules* **1985**, *18*, 2486.
(64) Zin, W. C.; Roe, R. J. *Macromolecules* **1984**, *17*, 183.
(65) Roe, R. J.; Zin, W. C. *Macromolecules* **1984**, *17*, 189.
(66) Owens, J. N.; Gancarz, I. S.; Koberstein, J. T.; Russell, T. P. *Macromolecules* **1989**, *22*, 3388.
(67) Hashimoto, T.; Tanaka, H.; Hasegawa, H. *Macromolecules* **1990**, *23*, 4378.
(68) Tanaka, H.; Hasegawa, H.; Hashimoto, T. *Macromolecules* **1991**, *24*, 240.
(69) Green, P. F.; Russell, T. P.; Jérôme, R.; Granville, M. *Macromolecules* **1989**, *22*, 908.
(70) Whitmore, M. D.; Noolandi, J. *Macromolecules* **1985**, *18*, 657.
(71) Leibler, L.; Orland, H.; Wheeler, J. C. *J. Chem. Phys.* **1983**, *79*, 3550.
(72) Leibler, L. *Makromol. Chem., Macromol. Symp.* **1988**, *16*, 1.
(73) Selb, J.; Marie, P.; Rameau, A.; Duplessix, R.; Gallot, Y. *Polym. Bull.* **1983**, *10*, 444.
(74) Rigby, D.; Roe, R. J. *Macromolecules* **1984**, *17*, 1778; **1986**, *19*, 721.
(75) Kinning, D. J.; Thomas, E. L.; Fetters, L. J. *J. Chem. Phys.* **1990**, *90*, 5806; *Macromolecules* **1991**, *24*, 3893.
(76) Banaszak, M.; Whitmore, M. D. *Macromolecules* **1992**, *25*, 249.
(77) Shull, K. R.; Kramer, E. J. *Macromolecules* **1990**, *23*, 4769.
(78) Noolandi, J. *Polym. Eng. Sci.* **1984**, *24*, 70.
(79) Noolandi, J.; Hong, K. M. *Macromolecules* **1982**, *15*, 482; **1984**, *17*, 1531.
(80) Vilgis, T. A.; Noolandi, J. *Macromolecules* **1990**, *23*, 2941; *Makromol. Chem., Macromol. Symp.* **1988**, *16*, 225.
(81) Brown, H. R. *Macromolecules* **1989**, *22*, 2859.
(82) Cho, K.; Brown, H. R.; Miller, D. C. *J. Polym. Sci., Polym. Phys. Ed.* **1990**, *28*, 1699.
(83) Koberstein, J. T.; Morra, B.; Stein, R. S. *J. Appl. Crystallogr.* **1980**, *13*, 34.
(84) Porod, G. *Kolloid Z.* **1951**, *124*, 83; **1952**, *125*, 51, 108.
(85) Rathje, J.; Ruland, W. *Colloid Polym. Sci.* **1976**, *254*, 358.
(86) Wiegand, W.; Ruland, W. *Prog. Colloid Polym. Sci.* **1979**, *66*, 355.
(87) Ruland, W. *Colloid Polym. Sci.* **1977**, *255*, 417.
(88) Bonart, R.; Muller, E. H. *J. Macromol. Sci., Phys.* **1974**, *B10*, 177.
(89) Vonk, C. G. *J. Appl. Crystallogr.* **1973**, *6*, 81.
(90) Ruland, W. *J. Appl. Crystallogr.* **1971**, *4*, 70.
(91) Lake, J. A. *Acta Crystallogr.* **1967**, *23*, 191.
(92) Vonk, C. G. *J. Appl. Crystallogr.* **1971**, *4*, 340; **1975**, *8*, 340.
(93) Glatter, Q. *J. Appl. Crystallogr.* **1974**, *7*, 147; **1977**, *10*, 415; *Acta Phys. Austriaca* **1977**, *47*, 83.
(94) Deutsch, M.; Luban, M. *J. Appl. Crystallogr.* **1978**, *11*, 87, 98; **1980**, *13*, 233.
(95) Walter, G.; Schmidt, P. W. *J. Appl. Crystallogr.* **1981**, *14*, 28.
(96) Guinier, A.; Fournet, G. *Small Angle Scattering of X-Rays*, Wiley: New York, 1955.
(97) Ruland, W. *J. Appl. Crystallogr.* **1974**, *7*, 383.
(98) Perrin, P. Ph.D. Thesis, Laval University, 1992.
(99) Hendricks, R. W.; Schmidt, P. W. *Acta Phys. Austriaca* **1967**, *26*, 97; **1973**, *37*, 20.
(100) Hendricks, R. W. *Program Weight: A Fortran IV Program for Evaluation of Weighting Function Used in SAXS*; USAEC Report ORNL-TM-1950 (Rev. 2); Oak Ridge National Laboratory: Oak Ridge, TN, 1972.
(101) Scientific Subroutine Package, Version 3, Programmer's manual; IBM: New York, 1968.
(102) Yukioka, S.; Inoue, T. *Polymer* **1982**, *34*, 1256.
(103) Kressler, J.; Higashida, N.; Inoue, T.; Heckman, W.; Seity, F. *Macromolecules* **1993**, *26*, 2090.
(104) Huttenbach, S.; Stamm, M.; Reiter, G.; Foster, M. *Langmuir* **1991**, *7*, 2438.
(105) Zhao, W.; Zhao, X.; Rafailovich, M. H.; Sokolov, J.; Mansfield, T.; Stein, R. S.; Composto, R. C.; Kramer, E. J.; Jones, R. A. L.; Sansone, M.; Nelson, M. *Physica B* **1991**, *173*, 43.
(106) Ballard, D. G. H.; Wignall, G. D.; Schelten, J. *Eur. Polym. J.* **1973**, *9*, 965.
(107) Kirste, R. G.; Kratky, O. *Z. Phys. Chem.* **1962**, *31*, 383.
(108) Kirste, R. G. *Makromol. Chem.* **1967**, *101*, 91.
(109) McMaster, L. P. *Macromolecules* **1973**, *6*, 760.
(110) Rogers, S. S.; Mandelkern, L. *J. Phys. Chem.* **1957**, *61*, 985.
(111) Paul, D. R.; Newman, S. *Polymer Blends*; Academic Press: New York, 1978; Vol. 2, Chapter 12.